Supporting Material

Single-molecule visualization of the oligomer formation of the non-hexameric *Escherichia coli* UvrD helicase

Hiroaki Yokota[†,‡,*], Yuko Ayabe Chujo[§], and Yoshie Harada[†]

[†]Institute for Integrated Cell-Material Sciences (WPI-iCeMS), Kyoto University, Yoshida-Honmachi, Sakyo-ku, Kyoto 606-8501, Japan.

[‡]PRESTO, Japan Science and Technology Agency, Gobancho Building 5F, 7, Gobancho, Chiyoda-ku, Tokyo, 102-00764, Japan.

[§]Department of Medical Genome Sciences, The University of Tokyo, 5-1-5 Kashiwanoha, Kashiwa, Chiba 277-8561, Japan.

[*]To whom correspondence should be addressed. E-mail: hyokota@icems.kyoto-u.ac.jp

Supplementary Materials and Methods

Buffers

The buffers, which are shown in Table S1, were prepared with reagent grade chemicals and deionized water, which was obtained through the use of a Milli-Q system (Merck Millipore, Darmstadt, Germany).
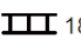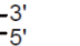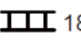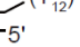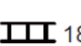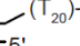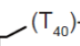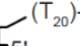
TABLE S1 Buffers

Buffer	Content
Buffer U	6 mM NaCl, 2.5 mM $MgCl_2$, 10% (v/v) glycerol, and 25 mM Tris-HCl (pH 7.5)
Annealing buffer	50 mM NaCl, 2 mM $MgCl_2$, and 20 mM Tris-HCl (pH 7.4)
Resuspension buffer	10% (w/v) sucrose and 50 mM Tris-HCl (pH 8.0)
Binding buffer	500 mM NaCl, 5 mM imidazole, 10% (v/v) glycerol, 20 mM Tris-HCl (pH 7.9)
Wash buffer	500 mM NaCl, 64 mM imidazole, 10% (v/v) glycerol, and 20 mM Tris-HCl (pH 7.9)
0-M NaCl buffer	10% (v/v) glycerol and 20 mM HEPES (pH 7.0)
200-mM NaCl buffer	200 mM NaCl, 10% (v/v) glycerol, and 20 mM HEPES (pH 7.0)
500-mM NaCl buffer	500 mM NaCl, 10% (v/v) glycerol, and 20 mM HEPES (pH 7.0)
Digestion buffer	0.05% (w/v) sodium dodecyl sulfate (SDS) and 50 mM sodium phosphate (pH 8.0)

DNA substrates

The sequence of the top strand of the duplex oligonucleotides that were used for the DNA binding and unwinding assays and single-molecule imaging experiments, which are shown in Table S2, is 5′-TGGCGACGGCAGCGAGGC-3' (1-5). The duplex DNA substrates were prepared through hybridization reactions that were performed by heating the oligonucleotide mixture, which was dissolved in annealing buffer, at 95 °C for 10 min and then cooling it to 30 °C at a rate of −0.25 °C/min using a thermal cycler. After 12.5% (w/v) polyacrylamide/TBE (Tris/Borate/EDTA) gel electrophoresis was performed to remove the non-hybridized oligonucleotides, the bands corresponding to the duplex DNA substrates were excised, eluted by electrophoresis and stored in the form of aliquots at −20 °C until use.

TABLE S2 DNA substrates

Substrate	Duplex length (bp)	3' ssDNA tail length (nt)	Structure
I	18	0	3'-Biotin 5' ▭▭▭ 18 ▭▭▭ 3'/5'
II	18	12	5'-Cy3 / 3'-Biotin ▭▭▭ 18 ▭▭▭ (T$_{12}$)-3' / 5'
III	18	20	3'-Biotin 5'- ▭▭▭ 18 ▭▭▭ (T$_{20}$)-3' / 5'
IV	18	40	3'-Biotin 5'- ▭▭▭ 18 ▭▭▭ (T$_{40}$)-3' / 5'
V	18	20	5'-Cy3 / 3'-Biotin ▭▭▭ 18 ▭▭▭ (T$_{20}$)-3' / 5'

The sequence of the top strand of the duplex oligonucleotides is 5′-TGGCGACGGCAGCGAGGC-3'.

The sequences of the oligonucleotides used for the Cys-Ala site-directed mutagenesis are the followings: UvrDC52A-F, 5'-<u>GCA</u>TCGCCATACTCGATTATGGCGGTGACG-3'; UvrDC52A-R, 5'-GTTTTCCACGCTCATCAACCAGGC-3'; UvrDC640A-F, 5'-<u>GCA</u>GTGGAAGAGGTGCGCCTGCGCGCC-3'; and UvrDC640A-R, 5'-CTCTTCCGGCAGCTCGCCGAT-3'. The underlined sequences were designed for site-directed mutagenesis.

UvrD proteins

The full coding region of the *uvrD* gene, which was subcloned into the His-tagged vector pET-15b, was a generous gift from Xu Guang Xi (5-7). The Cys-to-Ala mutations were introduced through site-directed mutagenesis using UvrDC52A-F, UvrDC52A-R, UvrDC640A-F, and UvrDC640A-R.

E. coli BL21 (DE3) cells harboring the constructed vector, in which the expression of the His-tagged *uvrD* gene to be expressed was under the control of the T7 promoter, were used for the expression of this protein. LB medium with 50 µg/ml ampicillin was inoculated with the pre-cultured BL21 (DE3) cells (at a final OD$_{550}$ of 0.004) and then incubated at 37 °C. When the OD$_{600}$ reached 0.4–0.6, IPTG was added to the medium to a final concentration of 0.1 mM. The cells were then incubated at 37 °C for 4 h, harvested by centrifugation at 5,000 rpm (3,900

× *g*) for 5 min at 4 °C and washed through two cycles of suspension in resuspension buffer and centrifugation to remove all of the LB. The cells were then homogenized in binding buffer by ultrasonication for 10 min on ice. The crude extract was obtained from the homogenized cells by ultracentrifugation at 15,000 rpm (29,300 × *g*) for 60 min at 4 °C.

The overexpressed UvrD protein in the crude extract was purified at 4 °C under native conditions by hexa-histidine tag affinity chromatography using an FPLC system (ÄKTAexplorer 10 S, GE Healthcare). First, the crude extract was filtered through a syringe filter with a 0.45-µm pore size and applied to a Ni^{2+}-charged HisTrap HP 1 ml column (GE Healthcare) at a 1 ml/min flow rate. The column was then washed with 5 ml of binding buffer and 5 ml of wash buffer at a 2 ml/min flow rate. The UvrD protein was eluted using a 30-ml linear imidazole gradient (64–154 mM). The elution was diluted with binding buffer to decrease the imidazole concentration to 55 mM and applied to a Co^{2+}-charged HisTrap HP 1 ml column. The Co^{2+}-charged column was washed with 5 ml of buffer containing 55 mM imidazole. The UvrD protein was then eluted with a 30-ml linear imidazole gradient (55–154 mM). The resultant elution was diluted with the 0-M NaCl buffer to decrease the NaCl concentration to 200 mM and then applied to a HiTrap heparin HP 1 ml column (GE Healthcare) that was pre-equilibrated with 200-mM NaCl buffer. The heparin column was then washed with 5 ml of 200-mM NaCl buffer, and the UvrD protein was eluted with a 5-ml linear NaCl gradient (0.2–1 M NaCl). The purity of the UvrD protein in the elution was verified by 12.5% SDS-polyacrylamide gel electrophoresis (PAGE) and the concentration was determined spectrophotometrically using $\varepsilon_{280} = 106,000$ cm^{-1}M^{-1} (8).

Fluorescence labeling of unmutated and mutated UvrD proteins

The fluorescence labeling of the purified UvrD proteins was performed with SH-reactive tetramethylrhodamine (TMR) maleimide (T6027, Molecular Probes, Grand Island, NY) or Cy5 maleimide (PA25001, GE Healthcare) at a UvrD:dye molar ratio of 1:3 in 500 mM NaCl buffer for 20 h at 4 °C. These dyes were chosen because the maleimide group reacts with cysteine residues with high specificity (9). The X-ray crystal structures (10) showed that three out of the six cysteine residues of the UvrD protein are exposed on the surface (Fig. S1). The unlabeled dyes were removed using a HiTrap heparin HP column. The labeling ratios were determined spectrophotometrically using the following extinction coefficients: $\varepsilon_{280} = 106,000$ cm^{-1} M^{-1} for the UvrD protein, $\varepsilon_{541} = 62,800$ cm^{-1} M^{-1} for TMR and $\varepsilon_{650} = 250,000$ cm^{-1}M^{-1} for Cy5. The calculations of the UvrD concentrations were corrected for the absorbance of the dyes at 280 nm (20% of the absorbance at 541 nm for TMR and 5% of the absorbance at 650 nm for Cy5). The labeled UvrD proteins were aliquoted, quickly frozen in liquid nitrogen and stored at −80 °C.

Identification of fluorescently labeled cysteine residues

To determine which cysteine residues were labeled, we digested TMR- or Cy5-labeled unmutated UvrD protein with endoproteinase Asp-N, which cleaves peptide bonds on the N-terminal side of aspartic and cysteic acid residues (11). The complete digestion by Asp-N distributes the six cysteine residues among different peptides. The cysteine residues (their corresponding molecular weights and the N-terminal amino acid sequences of the peptides) are Cys52 (10.1 kDa, DKQRE), Cys181 (3.7 kDa, DEGLR), Cys322 (1.6 kDa, DGEPI), Cys350 (5.5 kDa, DNGGA), Cys441 (3.9 kDa, DRQLT) and Cys640 (9.3 kDa, DEGGR). The purified TMR-or Cy5-unmutated UvrD protein was mixed with an equal volume of acetone, incubated at −80 °C for 12 h, and precipitated by ultracentrifugation at 15,000 rpm (29,300 × g) for 20 min at 4 °C. The precipitation was suspended in digestion buffer at 37 °C and digested by Asp-N (11420488, Roche, Basel Switzerland) at 37 °C for 16 h. The ratio (w/w) of UvrD to Asp-N in the digestion reaction was 10:1. The digestion reaction was verified by 12.5% Tricine-SDS PAGE. Several bands corresponding to the digested peptides were detected in the Coomassie brilliant blue (CBB)-stained gel, although the major fluorescence was detected only in the 10-kDa peptide bands that corresponded to both the TMR-UvrD and Cy5-UvrD proteins.

The digested peptides from the TMR-UvrD protein were separated by reverse-phase high-performance liquid chromatography (HPLC) using the SMART micro-purification system (GE Healthcare). The digested peptides were filtered through a syringe filter with a 0.2-µm pore size and then applied to a µRPC C2/C18 column (2.1 × 100 mm, 17-5057-01, GE Healthcare). The peptides were eluted with 48 ml of a linear gradient of acetonitrile (20–45%) that was supplemented with 0.05% trifluoroacetic acid at a rate of 0.1 ml/min. The elution profile was monitored through the absorbances at 215 and 541 nm for the peptide and TMR, respectively. The fractions corresponding to the two major absorbance peaks at 541 nm were collected and analyzed as described below.

The separated peptides were concentrated by a centrifugal concentrator system (VC-15SP, TAITEC, Tokyo, Japan), subjected to 15% Tricine-SDS PAGE, electrotransferred to a polyvinylidene difluoride (PVDF) membrane (FluoroTrans W Membrane, NIPPON Genetics, Tokyo, Japan) and then stained with CBB. The PAGE analysis showed that the molecular weight (MW) of the peptides from the fractions was approximately 10 kDa and that the MW of the peptide in one of fractions was lower than that in the other fraction. The stained bands corresponding to the TMR-labeled peptides were cut from the PVDF membrane. The N-terminal amino acid sequences of the peptides were then analyzed by the APRO Life Science Institute (Naruto, Japan). The N-terminal amino acid sequences of the peptides were DKQRE and DEGGR, which demonstrates that Cys52 and Cys640 were the major cysteine residues that were fluorescently labeled. This makes sense because Cys52 and Cys640 are exposed on the

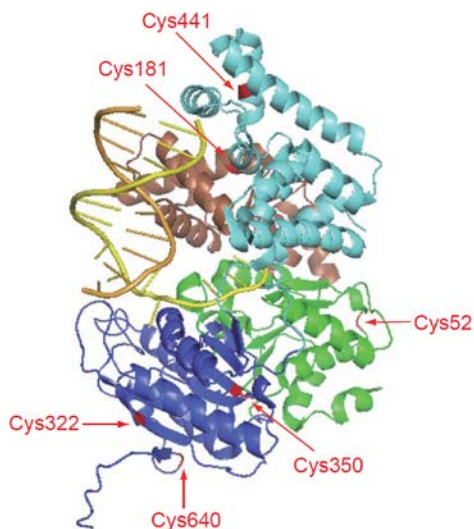surface (Fig. S1) and are thus likely susceptible to labeling.

FIGURE S1 Positions of the six cysteine residues of the UvrD protein in the UvrD–DNA complex. The crystal structure of the UvrD–DNA complex in the absence of nucleotide [Protein Data Bank (PDB) code: 2IS1] is shown as a ribbon diagram that was drawn using MacPyMol (http://delsci.com/macpymol/). The six cysteine residues are shown in red with their corresponding residual numbers. Domains 1A (1–89 and 215–280 amino acids), 1B (90–214 amino acids), 2A (281–377 and 551–647 amino acids) and 2B (378–550 amino acids) are shown in green, beige, blue and cyan, respectively.

PEGylation

The quartz slides (26 × 50 mm, thickness = 1 mm and 26 × 60 mm with two holes (1 mm in diameter), thickness = 1 mm, custom-made by Hikari-kobo, Tokyo, Japan) and silicate coverslips (18 × 18 mm, thickness = 0.12–0.17 mm, C218181 and 25 × 60 mm, thickness = 0.12–0.17 mm; C025601; Matsunami Glass, Osaka, Japan) were sonicated twice in 0.2 N KOH for 15 min and then in EtOH for 15 min. After each step, they were thoroughly rinsed with Milli-Q water. The PEG coating was performed as described previously with minor modifications (5). First, the cleaned glass substrates were amine-modified with 2% (v/v) *N*-2-(aminoethyl)-3-aminopropyl-triethoxysilane (KBE-603, Shin-Etsu Chemical, Tokyo, Japan) in stirred methanol containing 135 mM acetic acid and 4% (v/v) Milli-Q water for 20 min at room temperature. The amine-modified glass substrates were then washed with Milli-Q water and dried on a clean bench. A drop containing 10 mg (50 μl of 200 mg/ml) of PEG with an amine-reactive N-hydroxy-succinimidyl (NHS) group (SUNBRIGHT ME-50CS, MW = 5,000 Da, NOF Corporation, Tokyo, Japan) and 0.1 mg NHS-PEG-biotin (0H4M0H02, MW. = 5,000 Da, Nektar, USA or 13 5000-25-35, MW. = 5,000 Da, Rapp Polymere, Tuebingen, Germany)

dissolved in 50 mM MOPS (pH 7.5) was then placed on the surface of the quartz slides and 25 × 60-mm coverslips and covered by a rectangular-shaped (~20 × 20 mm) plastic film. The PEGylation reaction was performed for 3 h at room temperature. The surfaces of the 18 × 18-mm and 25 × 60-mm coverslips, which were used to make a flow cell, were coated with a drop containing 5 mg (25 µl of 200 mg/ml) and 10 mg (50 µl of 200 mg/ml) of PEG, respectively, that was dissolved in 50 mM MOPS (pH 7.5) on Parafilm for 3 h at room temperature. The PEGylated glass substrates were thoroughly rinsed with Milli-Q water, dried on a clean bench and stored at −80 °C in a vacuum until use.

Single-molecule imaging assays

All single-molecule experiments reported in this paper were performed at 25 °C using either of two types of flow cells. The two types of flow cells employed different total internal reflection fluorescence methods: a nail polish-sealed flow cell with prism-type total internal reflection microscopy or a double-sided tape-sealed flow cell with objective-type total internal reflection microscopy.

(i) The assays conducted using the nail polish-sealed flow cell with prism-type total internal reflection microscopy (Fig. 1 *A*)

The assays were performed in a flow cell that was built using a 18 × 18 mm-PEG-coated coverslip and a 25 × 60 mm-biotin-PEG-coated quartz slide that were sandwiched by two strips of plastic film (thickness = 0.08 mm) and sealed with nail polish.

Before the assays, the flow cell was first washed with 50 µl of buffer U (6 mM NaCl, 2.5 mM MgCl$_2$, 10% (v/v) glycerol, and 25 mM Tris-HCl (pH 7.5)) and then with 50 µl of 1 mg/ml Pluronic F-127 (P2443, Sigma, St. Louis, MO) in buffer U to further reduce the non-specific adsorption of Cy5-UvrDC640A on the surface. The slide was coated with 50 µl of 0.1 mg/ml streptavidin in buffer U for 5 min. Then, 50 µl of 20 pM DNA substrate with biotin at one end in buffer U was infused and immobilized onto the quartz glass surface via streptavidin–biotin interactions. After each step in the procedure, the channel was flushed with 150 µl of buffer U to remove any unbound molecules in solution. A volume of 50 µl of the indicated concentration of Cy5-UvrDC640A in buffer U with an oxygen scavenger system (12) (4.5 mg/ml glucose (168-06, Nacalai Tesque, Kyoto, Japan), 0.036 mg/ml catalase (106810, Roche, Basel Switzerland), 0.216 mg/ml glucose oxidase (G-7016, Sigma), and 143 mM β-mercaptoethanol (214-38, Nacalai Tesque) was then infused. The plastic film was subsequently removed from the flow cell and sealed with nail enamel prior to the single-molecule fluorescence observations.

(ii) The assays conducted using the double-sided tape-sealed flow cell and objective-type total internal reflection microscopy (Fig. 3 *A*)

The assays were performed in a flow cell that was built by sandwiching a PEG-coated 26 × 60

mm-quartz slide having two holes (1 mm in diameter) for the inlet and outlet and a 25×60 mm-biotin-PEG-coated coverslip with a preformed piece of double-sided tape (thickness = 0.125 mm, 468MP, 3M, St. Paul, MN). Inlet and outlet ports (NanoPorts, Upchurch Scientific, Oak Harbor, WA) were attached to the holes using preformed adhesive rings (IVY9040CGP, Daikyo Giken-Kogyo, Sagamihara, Japan). A six-way selection valve (V-241, Upchurch Scientific) was attached to a needle port (#9013, Upchurch Scientific) and used to infuse solutions containing either Pluronic F-127, streptavidin, or a DNA substrate into the flow cell through syringe-loading injectors. A syringe pump (KDS210, KD Scientific, Holliston, MA) was used to control the delivery of buffer U to the flow cell, and a microsyringe pump (CXN1150, ISIS, Osaka, Japan) was used to control the delivery of Cy5-UvrDC640A solution to the cell. The recording of single-molecule fluorescence images was initiated just prior to the infusion of Cy5-UvrDC640A into the chamber.

Before the assays were performed, the flow cell was washed with 100 µl of buffer U and then filled with 100 µl of 1 mg/ml Pluronic F-127 in buffer U. The coverslip surface was subsequently coated with 100 µl of 0.1 mg/ml streptavidin in buffer U for 5 min. Then, 100 µl of 20 pM DNA substrate with biotin at one end in buffer U was infused and immobilized onto the glass surface via streptavidin–biotin interactions. After each procedure, the flow cell was flushed with 500 µl of buffer U to remove any unbound molecules in solution. A volume of 100 µl of 2 nM Cy5-UvrDC640A in buffer U with 1 mM ATP and an oxygen scavenger system (13) (2.5 mM protocateuic acid (168-05251, Wako Pure Chemical Industries, Tokyo, Japan), 250 nM protocatechuate dioxygenase (P8279, Sigma), and 2 mM Trolox (238813, Nacalai Tesque) was then infused into the flow cell at a rate of 50 µl/min.

Microscope

The prism-type and objective-type of total internal reflection microscopy was conducted using two identical inverted microscopes (IX71, Olympus, Tokyo, Japan).

In the experiments with prism-type total internal reflection microscopy, an Nd:YAG laser (Compass 215M, Coherent, Santa Clara, CA) and a diode laser (Cube 635-25C, Coherent, Santa Clara, CA), which were used to excite Cy3 at 532 nm and Cy5 at 637 nm, were incident on the sample plane. The fluorescence signals from the samples were collected by an objective (PlanApo $\times$ 100 NA = 1.40, Olympus), imaged using a dual-view apparatus, and recorded with an EBCCD video camera (C7190-23, Hamamatsu Photonics, Hamamatsu, Japan) coupled to an image intensifier (C9016-02, Hamamatsu Photonics, Hamamatsu, Japan) with a 33 millisecond time resolution.

In the experiments conducted using objective-type total internal reflection microscopy, an Nd:YAG laser (Compass 215M, Coherent, Santa Clara, CA) and a HeNe laser (Cube 635-25C,

CVI Melles Griot, Albuquerque, NM), which were used to excite Cy3 at 532 nm and Cy5 at 632.8 nm, were incident on the sample plane. In addition, to minimize photobleaching of the dyes, these lasers were simultaneously incident on the sample plane for 100 milliseconds every second with mechanical shutters (LS3, Uniblitz, Rochester, NY). The fluorescence signals from the samples were collected by an objective (PlanApo $\times$ 100 TIRFM NA = 1.45, Olympus), imaged using a dual-view apparatus and recorded with an electron multiplying CCD (EMCCD) camera (DU-860, Andor Technology, Belfast, UK) with a one-second time resolution using Andor IQ software. The recorded images were analyzed using Image-Pro PLUS (Media Cybernetics, Rockville, MD).

Supplementary Results

Supplementary Result 1:

Labeling ratios of the UvrD mutants

We created three Cys-Ala mutants (UvrDC52A, UvrDC640A and UvrDC52A/C640A) using site-directed mutagenesis and labeled them with TMR- or Cy5-maleimide to determine which Cys-Ala mutant (UvrDC52A or UvrDC640A) could be labeled with a higher specificity and a higher labeling ratio. The labeling ratios, which are shown in Table S3, of the Cy5-labeled UvrDC52A (9%) and UvrDC640A (75% or 90%) were higher than or the same as those obtained with the TMR-labeled UvrDC52A (30%) and UvrDC640A (75%). The labeling ratios for the double mutant, UvrDC52A/C640A, were 15% with TMR and 10% with Cy5. These results suggest that Cys52 is more reactive with the dyes than Cys640 and that 10% of the labeling was obtained through the labeling of UvrD residues other than Cys52 and Cys640.

TABLE S3 Labeling ratios of the fluorescently labeled UvrD proteins

Cys mutation(s)	TMR (%)	Cy5 (%)
None	90	120
C52A	30	9
C640A	75	75 or 90
C52A/C640A	15	10

Supplementary Result 2:

DNA binding and unwinding activities of the labeled UvrD proteins

To check DNA binding and unwinding activities of the labeled UvrD proteins, we performed DNA binding and unwinding assays as previously described (14) with some modifications (Fig. S2 *A*) using a Cy3-labeled 18-bp dsDNA with a 20-nt 3' ssDNA tail (substrate V; Table S2) and analyzed the products by 12.5% (w/v) polyacrylamide/Tris/Borate/EDTA (TBE) gel electrophoresis. For the DNA binding assay, the UvrD (140 nM) protein was mixed with the DNA substrate (70 nM) and incubated in buffer U for 10 min at 37 °C. For the DNA unwinding assay, ATP (1 mM of final concentration) was added to the above incubated mixture and incubated for an additional 2 min at 37 °C. The reactions were quenched by rapid cooling on ice. The products were subjected to 12.5% (w/v) polyacrylamide/TBE gel electrophoresis and analyzed using a laser-excited fluorescence gel scanner (PharosFX, Bio-Rad Laboratories). Fig. S2 *B* shows the Cy3 fluorescence images of the gels. The TMR- and Cy5-labeled unmutated UvrD proteins and the TMR- and Cy5-labeled UvrDC640A exhibited the same DNA binding and unwinding activities as the unlabeled UvrD protein. The data for Cy5-UvrDC52A are not

shown because it lost DNA binding capability and was therefore not purified by a heparin column.

Thus, we chose to use Cy5-UvrDC640A among the fluorescently labeled mutants for our single-molecule imaging assays for the following three reasons: (i) its labeling ratio was the highest among the fluorescently labeled mutants; (ii) it retained its DNA binding and unwinding activities; and (iii) the non-specific labeling ratio of Cy5-UvrDC640A was lower than that of TMR-UvrDC640A.
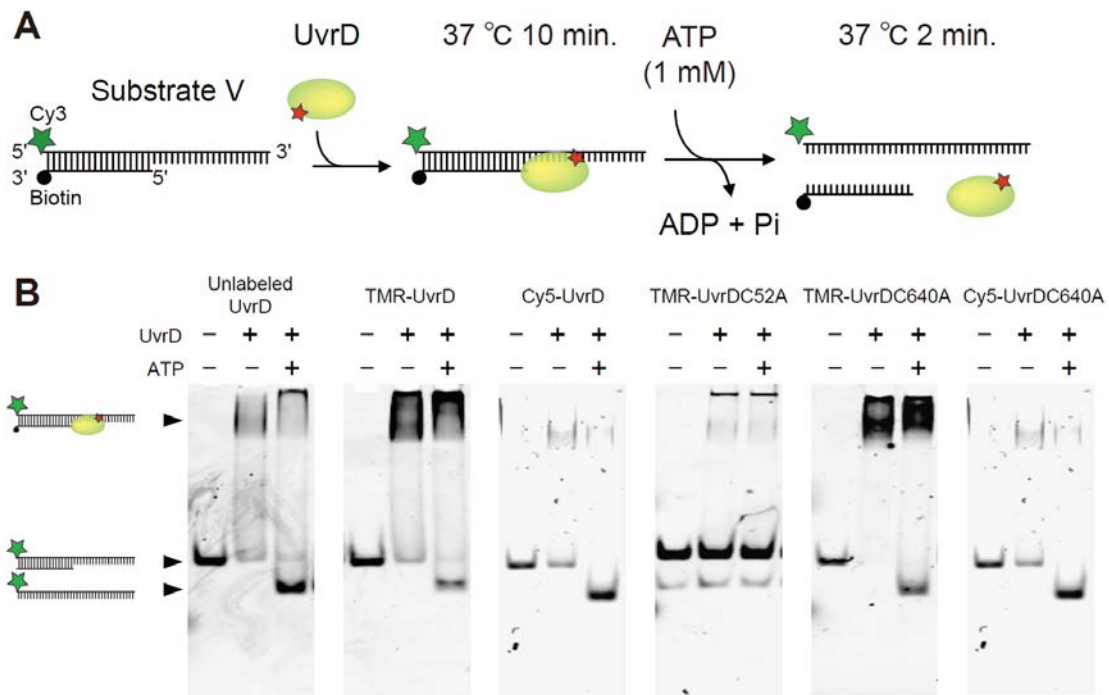
FIGURE S2 DNA binding and unwinding activities of the labeled UvrD proteins. (*A*) Schematic representation of the assays. For the DNA binding assays, the UvrD protein (140 nM) was mixed with 18-bp dsDNA with a 20-nt 3' ssDNA tail with a biotin at one end and Cy3 at the other end (substrate V, Table S2; 70 nM) and incubated in buffer U for 10 min at 37 °C. For the DNA unwinding assay, ATP (at a final concentration of 1 mM) was added to the incubated mixture and incubated for an additional 2 min at 37 °C. To evaluate the protein activities, we analyzed the Cy3 fluorescence of the end products through 12.5% (w/v) polyacrylamide/TBE gel electrophoresis using a fluorescence gel scanner. (*B*) Fluorescence images of the gels. The bands corresponding to the DNA substrate V, unwound Cy3-ssDNA and UvrD-bound substrate V are indicated by arrows.

Supplementary Result 3:

UvrD concentration required for efficient DNA unwinding in single-molecule imaging assays

To determine the Cy5-UvrDC640A concentration required for efficient DNA unwinding in single-molecule imaging assays, we determined the unwinding efficiency of different concentrations of Cy5-UvrDC640A (0.5, 1.0, or 2.0 nM) in the presence of 1 mM ATP and the Cy3-labeled 18-bp dsDNA with a 20-nt 3' ssDNA tail (substrate V, Table S2) that was immobilized on a quartz slide using prism-type total internal reflection fluorescence microscopy (detailed in Methods). The unwinding of the DNA substrate by the Cy5-UvrDC640A protein produced free Cy3-labeled ssDNA that diffused away from the surface, which allowed us to determine the Cy5-UvrDC640A concentration required for efficient DNA unwinding by observing the number of Cy3-fluorescent spots (Fig. S3 *A*). These fluorescent spots were then quantified and are shown in bar graph in Fig. S3 *B*. Almost no fluorescent spots were observed in either channel in the absence of the DNA substrate. In contrast, in the presence of the immobilized DNA substrate on the surface, many fluorescent spots were observed in the Cy3 channel. The addition of Cy5-UvrDC640A increased the number of Cy5 spots but did not decrease the number of Cy3 spots in the absence of ATP, which shows that Cy5-UvrDC640A bound to the DNA but did not unwind it. In the presence of Cy5-C640A and 1 mM ATP, the number of Cy3 fluorescent spots decreased as the Cy5-UvrDC640A concentration increased. Most of the Cy3 fluorescent spots disappeared in the presence of 1.0 or 2.0 nM Cy5-UvrDC640A, which indicates that a concentration of 1.0 nM of Cy5-UvrDC640A is sufficient for efficient DNA unwinding in our single-molecule imaging assays.
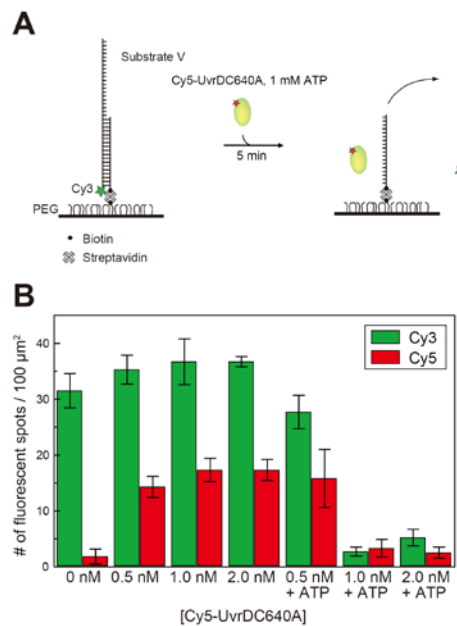
FIGURE S3 Determination of the Cy5-UvrDC640A concentration that is required for effective DNA unwinding in single-molecule imaging assays. (*A*) Schematic representation of the DNA unwinding assay. First, 18-bp dsDNA substrate with a 20-nt ssDNA tail, Cy3 at the 5' end of one strand and biotin at the 3' end of the other strand (substrate V, Table S2) was immobilized by streptavidin on a PEGylated quartz slide via streptavidin–biotin interactions. Then, 50 µl of buffer U containing the indicated concentration of Cy5-UvrDC640A and 1 mM ATP was infused into the flow cell. The number of Cy3 fluorescent spots decreased due to DNA unwinding by Cy5-UvrDC640A because the Cy3-ssDNA was released and diffused away from the surface. (**b**) Histogram of the number of fluorescent spots observed per 100 µm^2.

Supplementary Result 4:
Distribution of the number of Cy5 labels in the UvrDC640A proteins

We estimated the number of labeled Cy5 dyes per UvrDC640A molecule. We used the labeling ratios of Cy5-UvrDC640A (75 and 90%) and Cy5-UvrDC52A/C640A (10%) to calculate the distribution of the number of labels per protein.

First, we calculated the distribution of the number of Cy5 labels in the UvrDC52A/C640A protein. For this calculation, we assumed that certain amino acid residues of UvrDC52A/C640A, other than Ala52 and Ala640, were randomly labeled. The molar ratios of the UvrDC52A/C640A proteins that were labeled with different numbers of Cy5 molecules and the product of the number of Cy5 labels and the molar ratio are listed below, where a refers to the molar ratio of the UvrDC52A/C640A protein that was labeled with a single Cy5 molecule.

Number of labeled Cy5 labels	Molar ratio	Number of Cy5 labels × Molar ratio
0	$1 - \sum_{n=1}^{\infty} a^n = \dfrac{1-2a}{1-a}$	0
1	a	a
2	a^2	$2a^2$
3	a^3	$3a^3$
n	a^n	na^n
Total	1	$\sum_{n=0}^{\infty} na^n = \dfrac{a}{(1-a)^2}$

We obtained $a = 8.4 \times 10^{-2}$ by solving the equation $\sum_{n=1}^{\infty} na^n = \dfrac{a}{(1-a)^2} = 0.10$.

Substituting this value of a in the cases where the number of Cy5 labels was ≤ 3 yields the following:

Number of Cy5 labels	Molar ratio	Number of Cy5 labels × Molar ratio
0	0.91	0
1	8.4×10^{-2}	8.4×10^{-2}
2	7.0×10^{-3}	1.4×10^{-2}
3	5.9×10^{-4}	1.8×10^{-3}

We then calculated the molar ratios for the UvrDC640A proteins that were labeled with different amounts of Cy5 molecules using b as the specific labeling ratio of Cy5 to the Cys52 residue of the UvrDC640A protein; in this calculation, the value of b, which was assumed to be 0.65 or 0.80, was derived from the subtraction of the labeling ratio obtained for Cy5-UvrDC52A/C640A (10%) from the labeling ratio obtained for Cy5-UvrDC640A (75% or 90%). The molar ratios of the UvrDC640A proteins that were labeled with n Cy5 molecule(s) are described as r_n.

Number of labeled Cy5	Molar ratio
0	$r_0 = \dfrac{1 - 2a}{1 - a}(1 - b)$
1	$r_1 = \dfrac{1 - 2a}{1 - a}b + a(1 - b)$
2	$r_2 = ab + a^2(1 - b)$
3	$r_3 = a^2 b + a^3(1 - b)$
4	$r_4 = a^3 b + a^4(1 - b)$
…	…
n	$r_n = a^{n-1}b + a^n(1 - b)$
Total	1

The estimated molar ratios of the UvrDC640A proteins that were labeled with n Cy5 molecules ($n \leq 3$) are shown in Table S4.

TABLE S4 Estimate of the molar ratios of UvrDC640A proteins that were labeled with different numbers of Cy5 molecules

Number of Cy5 labels per UvrDC640A molecule	Molar ratio	
	75%	90%
0	0.32	0.18
1	0.62	0.74
2	5.7×10^{-2}	6.9×10^{-2}
3	4.8×10^{-3}	5.8×10^{-3}

Supplementary Result 5:

Predicted distributions of photobleaching steps

Based on the molar ratios for the UvrDC640A proteins that were labeled with different numbers of Cy5 molecules (labeling ratio = 75%), we predicted the distributions of the number of photobleaching steps (one, two, three and more than three) for the monomer, dimer, trimer, and tetramer models (Fig. 2 *C*).

Monomer model

The molar ratio for each step is the same as the molar ratio of UvrDC640A proteins that were labeled with n Cy5 molecules. The normalized molar ratio for each step is

$$\text{one step:two steps:three steps:more than three steps} = r_1 : r_2 : r_3 : 1 - \sum_{n=0}^{3} r_n = 0.91 : 8.4 \times 10^{-2} : 7.0$$

$\times\ 10^{-3} : 6.4 \times 10^{-4}$, where r_n is the molar ratio of UvrDC640A proteins that were labeled with n Cy5 molecules.

Dimer model

The molar ratio for each step can be calculated as the sum of the product(s) of two molar ratios of UvrDC640A proteins that are labeled with different numbers of Cy5 molecules and the combination $_nC_k$ ($= n!/r!(n-r)!$).

Zero steps: $r_0^2 \times\ _2C_2 = 0.10$

One step: $r_0 \times r_1 \times\ _2C_1 = 0.39$

Two steps: $r_0 \times r_2 \times\ _2C_1 + r_1^2 \times\ _2C_2 = 0.42$

Three steps: $r_0 \times r_3 \times\ _2C_1 + r_1 \times r_2 \times\ _2C_1 = 7.3 \times 10^{-2}$

More than three steps: $1 - \sum_{n=0}^{3} r_n = 1.1 \times 10^{-2}$

The normalized molar ratio for each step is therefore

one step:two steps:three steps:more than three steps $= 0.44 : 0.47 : 8.2 \times 10^{-2} : 1.2 \times 10^{-2}$.

Trimer model

The molar ratio for each step can be calculated as the sum of the product(s) of three molar ratios of UvrDC640A proteins that are labeled with different numbers of Cy5 molecules and $_nC_k$.

Zero steps: $r_0^3 \times\ _3C_3 = 3.2 \times 10^{-2}$

One step: $r_0^2 \times r_1 \times\ _3C_2 = 0.19$

Two steps: $r_0^2 \times r_2 \times\ _3C_2 + r_0 \times r_1^2 \times\ _3C_1 = 0.38$

Three steps: $r_0^2 \times r_3 \times\ _3C_2 + r_1^3 \times\ _3C_3 + r_0 \times r_1 \times r_2 \times\ _3C_1 \times\ _2C_1 = 0.24$

More than three steps: $1 - \sum_{n=0}^{3} r_n = 0.16$

The normalized molar ratio for each step is therefore

one step:two steps:three steps:more than three steps = 0.19:0.40:0.25:0.16

Tetramer model

The molar ratio for each step can be calculated as a sum of the product(s) of four molar ratios of UvrDC640A proteins that are labeled with different numbers of Cy5 molecules and $_nC_k$.

Zero steps: $r_0{}^4 \times {}_4C_4 = 1.0 \times 10^{-2}$

One step: $r_0{}^3 \times r_1 \times {}_4C_3 = 8.0 \times 10^{-2}$

Two steps: $r_0{}^3 \times r_2 \times {}_4C_3 + r_0{}^2 \times r_1{}^2 \times {}_4C_2 = 0.24$

Three steps: $r_0{}^3 \times r_3 \times {}_4C_3 + r_0{}^2 \times r_1 \times r_2 \times {}_4C_2 \times {}_2C_1 + r_0 \times r_1{}^3 \times {}_4C_1 = 0.35$

More than three steps: $1 - \sum_{n=0}^{3} r_n = 0.32$

The normalized molar ratio for each step is therefore

one step:two steps:three steps:more than three steps = 8.1×10^{-2}:0.24:0.35:0.33

Supplementary Result 6:

The goodness-of-fit tests

To test which model best fits the distributions of the number of photobleaching steps, we calculated their respective χ^2 values (Fig. S4), which represent the difference between observed and predicted distributions and were calculated with the equation.

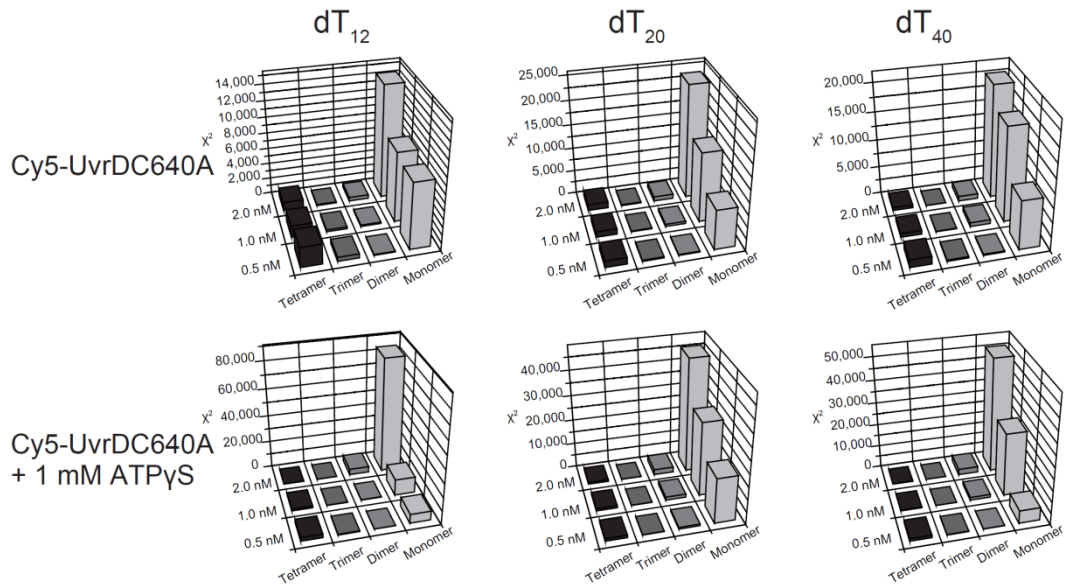$$\chi^2 = \sum_{i=1}^{n} \frac{(O_i - E_i)^2}{E_i}$$

FIGURE S4 χ^2 values for the goodness-of-fit tests. To test which model best fits the distributions, we calculated their χ^2 values, which represent the difference between observed and predicted distributions, using the equation that is shown in the text. The model that

minimizes the χ^2 value best fits the distribution. In all cases that were tested, χ^2 values of the monomer model were the highest.

where χ^2, O_i, E_i and n are the test statistic that asymptotically approaches a χ^2 distribution, the observed molar ratio for the i-step photobleaching, the predicted molar ratio for the i-step photobleaching that was calculated based on the null hypothesis, and the number of possible outcomes of each event, respectively. The model that minimizes the χ^2 value best fits the distribution.

Supplementary Result 7:

Predicted distributions of the number of Cy5 fluorescence step changes

Based on the molar ratios of the UvrDC640A protein with different numbers of Cy5 labels (labeling ratio = 90%), we estimated the ratios of zero-, one-, two-, three-, and four-step fluorescence changes for the monomer, dimer, trimer, and tetramer models (Fig. 3 *I*). All of the ratios were calculated using r_0, which is the molar ratio of the UvrDC640A protein that is labeled with zero Cy5 molecules (Table S4).

Monomer model

This model assumes that only a one-step fluorescence change can be observed. The normalized ratio for each step is zero step:one step:two steps:three steps:four steps = r_0:1− r_0:0:0 = 0.18:0.82:0:0.

Dimer model

Zero step: $r_0^2 \times {_2}C_2 = 0.033$

One step: $r_0 \times (1 - r_0) \times {_2}C_1 = 0.30$

Two steps: $(1 - r_0)^2 \times {_2}C_2 = 0.67$

The normalized ratio for each step that can be observed is

one step:two steps:three steps:four steps = 0.31:0.69:0:0.

Trimer model

Zero step: $r_0^3 \times {_3}C_3 = 6.0 \times 10^{-3}$

One step: $r_0^2 \times (1 - r_0) \times {_3}C_2 = 8.1 \times 10^{-2}$

Two steps: $r_0 \times (1 - r_0)^2 \times {_3}C_1 = 0.36$

Three steps: $(1 - r_0)^3 \times {_3}C_0 = 0.55$

The normalized ratio for each step that can be observed is

one step:two steps:three steps:four steps = 8.1×10^{-2}:0.36:0.54:0.

Tetramer model

Zero step: $r_0^4 \times {_4}C_4 = 1.1 \times 10^{-3}$

One step: $r_0^3 \times (1 - r_0) \times {_4}C_3 = 2.0 \times 10^{-2}$

Two steps: $r_0^2 \times (1 - r_0)^2 \times {_4}C_2 = 0.13$

Three steps: $r_0 \times (1 - r_0)^3 \times {}_4C_1 = 0.40$

Four steps: $(1 - r_0)^4 \times {}_4C_0 = 0.45$

The normalized ratio for each step that can be observed is

one step:two steps:three steps :four steps $= 2.0 \times 10^{-2}$:0.13:0.40:0.45.

TABLE S5 Comparison of the kinetic parameters determined in this study and in two previous studies

	This study	Bulk assay (Maluf *et al.*, 2003)	Single-molecule assay (Sun *et al.*, 2008)
k_1	0.063 ± 0.028 s^{-1} (138)	0.30 ± 0.04 s^{-1}	0.10 s^{-1}
k_2	0.10 ± 0.00 s^{-1} (123)	> 0.30 s^{-1}	0.15 s^{-1}
k_3	0.14 ± 0.07 s^{-1} (15)	–	–
k_4	0.064 ± 0.010 s^{-1} (25)	–	–
k_5	0.086 ± 0.047 s^{-1} (3)	–	–
k_6	0.085 ± 0.034 s^{-1} (6)	–	–
k_7	> 0.38 s^{-1} (60)	0.337 ± 0.016 s^{-1}	–
k_8	> 0.75 s^{-1} (6)	–	–
k_{-1}	0.20 ± 0.02 s^{-1} (82)	$< 0.025 \pm 0.005$ s^{-1}	0.12 s^{-1}
k_{-2}	0.40 ± 0.06 s^{-1} (77)	> 3 s^{-1}	–
k_{-3}	0.56 ± 0.20 s^{-1} (9)	–	–
k_{-4}	0.16 ± 0.03 s^{-1} (14)	–	–
k_{-5}	0.25 ± 0.14 s^{-1} (5)	–	–
k_{-6}	0.38 ± 0.16 s^{-1} (3)	–	–
k_{-7}	–	0.030 ± 0.006 s^{-1}	–
k_{-8}	–	–	–
K_1	$(1.6 \pm 0.9) \times 10^8$ M^{-1}	$(6.0 \pm 2.3) \times 10^9$ M^{-1}	4.2×10^8 M^{-1}
K_2	$(1.3 \pm 0.2) \times 10^8$ M^{-1}	$(4.9 \pm 0.7) \times 10^8$ M^{-1}	–
K_3	$(1.3 \pm 1.0) \times 10^8$ M^{-1}	–	–
K_4	$(2.1 \pm 0.7) \times 10^8$ M^{-1}	–	–
K_5	$(1.7 \pm 0.2) \times 10^8$ M^{-1}	–	–
K_6	$(1.1 \pm 0.9) \times 10^8$ M^{-1}	–	–
K_7	–	11.2 ± 2.3 M^{-1}	–
K_8	–	–	–

The rate constants obtained in this study using a single exponential fit are presented as the mean $\pm$ standard error (number of data points) except for k_3, k_5, k_6, k_{-3}, k_{-5}, and k_{-6}, which were obtained using only a small amount of data points, were determined through simple averaging and are presented as the mean $\pm$ standard deviation (number of data points). The lower limit of k_7 is the reciprocal of the dwell time of the second step of Cy5 fluorescence increase just before the unwinding of DNA for traces with two steps (2.7 ± 0.2 s). The lower limit of k_8 is the reciprocal of the dwell time of the step that corresponds to the UvrD trimer just before the DNA unwinding (2.3 ± 1.5 s). The dissociation constants obtained in the previous two studies are for

a UvrD concentration of 2 nM. The rate constants and equilibrium constants were calculated using the relationship: $K_n = k_{-n}/ (k_n \times 2 \times 10^{-9})$ ($n = 1$–4).

Supplementary Result 8:

Comparison of the rate constants of the sequential association (or dissociation) of two UvrD monomers and the association (or dissociation) of a UvrD dimer

The comparisons that are described in this section indicate that we are mostly visualizing the pre-assembled UvrD dimer association/dissociation in our assays.

(i) Comparison of the rate constants of the sequential association of two UvrD monomers (D→UD and UD→U$_2$D) and the association of a UvrD dimer (D→U$_2$D)

   The rate constants of the sequential association of two UvrD monomers (70 traces) are 0.077 ± 0.009 s^{-1} (D→UD) and 0.091 ± 0.011 s^{-1} (UD→U$_2$D), which are similar to the corresponding association rate constants shown in Fig. 5 *A* and Table S5. This result suggests that the rate of UvrD dimer formation through the sequential binding of two UvrD monomers is less than 0.05 s^{-1}. In contrast, the rate constant for the association of pre-assembled UvrD dimers with DNA (25 traces) is 0.064 ± 0.010 s^{-1}, which is comparable to the rate constant for the association of the first UvrD monomer with DNA (D→UD). These results suggest that the binding of UvrD dimers was visualized in this study because the probability that two UvrD monomers will sequentially bind to DNA in one second (8.7%) is much smaller than the probability of UvrD dimers binding to DNA in one second ($25/(70+25) = 26.3\%$).

(ii) Comparison of the rate constants of the sequential dissociation of two UvrD monomers (U$_2$D→UD and UD→D) and the dissociation of a UvrD dimer (U$_2$D→D)

   The same argument as above can be applied to the dissociation of a UvrD dimer (U$_2$D →D). The rate constants of the sequential dissociation of two UvrD monomers (29 traces) are 0.51 ± 0.07 s^{-1} (U$_2$D→UD) and 0.12 ± 0.01 s^{-1} (UD→D), which are similar to the corresponding association rate constants that are shown in Fig. 5 *A* and Table S5. This result suggests that the rate of UvrD dimer dissociation through the sequential dissociation of UvrD monomers is less than 0.1 s^{-1}. In contrast, the rate constant for the dissociation of UvrD dimers from DNA (14 traces) is 0.16 ± 0.03 s^{-1}, which is comparable to the rate constant for the dissociation of the second UvrD monomer from DNA (UD→D). These results suggest that the dissociation of UvrD dimers was visualized in this study because the probability that two UvrD monomers will sequentially dissociate from DNA in one second (11%) is much smaller than the probability of UvrD dimers dissociating from DNA in one second ($14/(29+14) = 33\%$).

Supplementary Discussions

Supplementary Discussion 1:

Effect of the UvrD concentration on the unwinding of DNA in single-molecule imaging assays

A series of biochemical studies by the Lohman group have suggested that the UvrD protein exhibits optimal helicase activity in an oligomeric form (1,3,4,15). They performed single-turnover DNA unwinding experiments using chemical quenched flow methods with varying UvrD and DNA concentrations under stoichiometric UvrD–DNA binding conditions. The quantitative analysis of their data indicated that a single UvrD monomer bound at the ss/dsDNA junction of any DNA substrate independently of the 3' ssDNA tail length. However, they found that a single UvrD monomer was not able to fully unwind even a short 18-bp duplex DNA and thus concluded that two UvrD monomers must interact with one another to form a functional helicase along the DNA. In our single-molecule imaging assays, the UvrD and DNA concentrations were lower than those in the single-turnover DNA unwinding experiments, i.e., the concentration of the DNA that was immobilized on a glass surface was on the order of pM (7.2 pM as estimated from the Cy3 fluorescent spot density) and the UvrD concentration was on the orders of nM. However, the binding of multiple UvrD proteins to the DNA was observed when the UvrD concentration was in molar excess of the DNA concentration. We assume that the high association rate constant and high UvrD equilibrium constant enabled us to observe the UvrD–DNA interaction at lower UvrD and DNA concentrations. The average time for the first UvrD monomer to bind to DNA after the UvrD protein was infused into the sample chamber was 18 ± 2 s. This time corresponds to a rate constant of 0.055 ± 0.005 s^{-1}, which is comparable to the association rate constant k_1 that was obtained in this study (Fig. 5 *A* and Table S5). The equilibrium constants K_1 and K_2, which were calculated using the corresponding rate constants, were $(1.6 \pm 0.9) \times 10^8$ M^{-1} and $(1.3 \pm 0.2) \times 10^8$ M^{-1}, respectively (Table S5). These K_1 and K_2 values, which were obtained at a temperature of 25 °C in buffer U with NaCl (6 mM) and glycerol (10% (v/v)), are comparable to the K_1 value that was obtained by Sun *et al.* (16) at 25 °C in a buffer containing NaCl (50 mM) and no glycerol (0% (v/v)) and to the K_2 value that was obtained by Maluf *et al.* (4) at 25 °C in a buffer that contained NaCl (20 mM) and glycerol (20% (v/v)), respectively. A study that used analytical ultracentrifugation (2) to investigate the self-association of the UvrD protein in buffers with higher NaCl concentration (20–500 mM) and glycerol contents (15–40% (v/v)) revealed that >95% of the UvrD proteins are found as monomers in 20 mM NaCl and 20% (v/v) glycerol at a UvrD concentration of 10 nM, which is higher than the UvrD concentrations used in this study (0.5, 1.0 and 2.0 nM) and is supported by a pre-steady state kinetics formation study (4). Thus, most of the UvrD protein is likely to be

monomeric at concentrations that are on the order of nM even in buffer U (6 mM NaCl and 10% (v/v) glycerol). The unwound fraction of DNA with a 20-nt 3' ssDNA tail was more than 80% in the presence of 1.0 or 2.0 nM UvrD protein (Fig. S3 *C*), which was more than 100 times the molar excess of DNA. The minimum UvrD concentration required for efficient DNA unwinding is similar to that determined in a single-molecule DNA manipulation study by Sun *et al* .(16), but different from that determined by Dessinges *et al.* (6), who used 0.25 nM UvrD. It is likely that the difference is due to larger sample volume of the glass capillary (1 × 1 mm cross section), which makes total number of UvrD proteins greater than the amount that was used in this study. An unwinding efficiency of greater than 10% was obtained using a pre-steady-state, single-turnover chemical quenching method in which 1.0 nM UvrD and 0.5 nM DNA were pre-incubated for 1 min before the addition of 1 mM ATP and a DNA trap was used to prevent the UvrD proteins from rebinding to the DNA (4). We attribute the greater unwinding efficiency to the multiple DNA-unwinding events that occurred during the incubation time (~min) prior to the single-molecule observation. The marked difference in the unwinding efficiency between 0.5 and 1.0 nM may be due to the insufficient lifetime of a monomer–DNA complex to ensure the formation of a dimer on the DNA substrate because the dissociation of the first UvrD monomer is likely to occur ($1/k_{-1}$ = 4.9 s) before the second UvrD monomer binds to the DNA substrate ($1/k_2$ = 9.7 s). A non-linear relationship was observed between the UvrD concentration and the DNA unwinding efficiency in a single-turnover DNA unwinding experiment (3) and in a DNA unwinding experiment with single-molecule DNA manipulation, which supports the idea that the binding step becomes rate-limiting at low UvrD and DNA concentrations (1,4,16).

Supplementary Discussion 2:
Possible reasons for the discrepancy in the values of the rate constants
The discrepancy in the values of the rate constants may be due to unobserved isomerization processes, the presence of unlabeled UvrD proteins, and the possible degradation of the helicase activity by Cy5 labeling. The buffer contents, especially the presence of ATP because nucleotides can alter the UvrD conformation and modulate the UvrD–DNA interaction, may also account for the difference in the rate constants. The first step of the double-mixing quenched flow kinetics experiments prior to the second ATP addition step involves the mixing of the UvrD proteins with DNA in the absence of ATP. Maluf *et al.* (4) subsequently estimated the rate constants and the lower or upper limits by constraining a number of fitting parameters based on certain assumptions using the data from the first step. The differences in the NaCl and glycerol concentrations between the different buffers may also contribute to the differences. Our buffer had a lower [NaCl] of 6 mM than their buffer (10 mM Tris, pH 8.3, 20 mM NaCl, and 20% (v/v) glycerol), which would promote the formation of pre-assembled dimers and alter the

UvrD–DNA interaction. In their buffer, more than 99% of the UvrD proteins were reported to be monomeric (2).

Supplementary Discussion 3:

Estimate of the time required for a second UvrD monomer to translocate on the 3' dT$_{20}$-ssDNA tail and unwind the 18-bp dsDNA

We mentioned in the text that three kinetic steps are supposed to occur during the mean dwell time of the multiple UvrD bound states (2.7 ± 0.2 s (Fig. 3 *G*) or 2.3 ± 1.5 s) just before the DNA unwinding: the translocation of the latecoming UvrD protein(s) on the ssDNA to form a UvrD oligomer with the pre-bound protein(s), the isomerization of the non-productive oligomer to make it productive, and the unwinding of the DNA. We estimated the time required for the latecoming UvrD monomer to find the pre-bound protein(s) and unwind the 18-bp dsDNA to show that these two processes occur in less than 1 s and to support the hypothesis that the isomerization process consumes most of the dwell time. The latecoming UvrD monomer interacts with the pre-bound monomeric protein(s) through direct contact or through translocatoin along the 3' ssDNA tail in less than 0.1 s because UvrD monomers are known to perform ATP-dependent translocation along ssDNA with a biased 3' to 5' directionality at a translocation rate of ~190 nt/s and a processivity of 769 ± 1 nt (17-19). In addition, a functional UvrD oligomer must completely unwind the 18-bp dsDNA substrate in less than half a second without dissociating from it because the unwinding rate and the processivity are reported to be 68 ± 9 bp/s and is 40–50 bp (15), respectively.

  In conclusion, the time required for the latecoming UvrD monomer to find the pre-bound protein(s) and unwind the 18-bp dsDNA is less than 1 s. Because the dwell time that was estimated by Maluf *et al* .(4) is 1/0.337 s^{-1} = 3.0 s (Table S5), which is similar to the mean dwell time that was found in this study (Fig. 3 *G*), the above estimate supports the hypothesis that the isomerization process consumes most of the dwell time.

Supplementary Discussion 4:

DNA unwinding that is driven by pre-assembled UvrD dimers

We obtained traces (25 traces) indicating that a pre-assembled UvrD dimer unwinds DNA. Maluf *et al.* claimed that pre-assembled UvrD dimers are functional helicases that can unwind DNA in less than 50 ms without undergoing isomerization process on the DNA (4). They estimated the rate of active dimer formation on DNA directly from the pre-assembled UvrD dimer. This rate was determined to be (1.1 ± 0.2) × 10^8 M^{-1}s^{-1} (or (0.22 ± 0.04) s^{-1} with 2 nM UvrD protein (Table S5)), which is higher than that obtained in this study ((0.06 ± 0.01) s^{-1}). We observed that the dimer unwinds the DNA in (2.0 ± 1.9) s upon binding, which is as fast as the

formation of a UvrD dimer through the sequential binding of two monomers. However, we cannot determine whether the pre-assembled dimer can unwind DNA without undergoing isomerization through our single-molecule imaging assays due to the lack of the required time resolution and the low amount of data obtained in this study.

Supplementary Discussion 5:

Comments on the monomer model proposed by other groups

The single-molecule imaging assays in this study support the oligomeric model as the mechanism by which the UvrD protein unwinds DNA. This is in contrast to the monomeric model that was proposed based on the data obtained from genetic complementation assays (20). Mechanic *et al.* reported that a UvrD truncation mutant, UvrDΔ40C (40 amino acid residues have been deleted from the C terminus), which is supposed to function as a monomer *in vitro* in a buffer containing 200 mM NaCl and 20% (v/v) glycerol (pH 8.3) at 20 °C, could unwind DNA, leading to the conclusion that wild-type UvrD proteins must also function as a monomer. However, Maluf *et al* .(2) claimed that UvrDΔ40C may form a dimer because the experiment was performed in a solution with a low NaCl concentration (20 mM), in the absence of glycerol (0%), at a low pH (7.5), and at a high temperature (37 °C) (3). They also showed that a shorter UvrD truncation mutant, UvrDΔ73C, which has a C terminus in which 73 amino acid residues have been deleted, was still capable of forming a dimer in a buffer containing 20 mM NaCl but not in 200 mM NaCl. A monomeric model was also proposed based on a series of crystal structures of UvrDΔ40C-DNA complexes (10). These structures suggest that a two-part power stroke is performed by the monomeric UvrD protein through a combined wrench and inchworm mechanism that consists of an ATP-dependent domain rotation between domain 2A and the remaining three domains (1A, 1B and 2B) and a subsequent ssDNA translocation. It seems reasonable that the researchers were able to produce crystals of the monomeric UvrD–DNA complex because UvrDΔ40C was used and the ssDNA tail length of the DNA substrates that were used for crystallization were 7 or 8-nt, which is shorter than the length required for efficient DNA unwinding ($\geq$ 12 nt) (3).

Supplementary Discussion 6:

Active mechanism proposed for the unwinding of DNA by the UvrD protein

It is proposed that UvrD functions through an active mechanism in which the helicase actively unwinds the duplex using energy from ATP hydrolysis. The Lohman group used single-turnover unwinding experiments to demonstrate a sequence-independent constant step size of four to five base pairs for the UvrD-catalyzed DNA unwinding process (3,15). Manosas *et al.* utilized a single-molecule DNA unwinding experiment with magnetic tweezers and determined that the

ratio of the rate of the DNA unwinding (in base pairs) to the velocity of the translocation on ssDNA (in nucleotides) is ~1 (7). The active mechanism is different from the passive mechanism in which the helicase simply moves along the ssDNA in the 3' to 5' direction and waits until transient thermal fluctuations open the upstream duplex to bind to the ssDNA that is formed.

Supplementary Discussion 7:

Implications of the mechanisms of SF1 DNA helicases

As with UvrD, the number of helicase molecules that are involved in the DNA unwinding also remains controversial for a number of other SF1 helicases, such as the *E. coli* Rep and *B. stearothermophilus* PcrA. These enzymes all consist of four subdomains: 1A, 1B, 2A, and 2B. The 1A and 2A subdomains in all of these proteins are responsible for ATP hydrolysis, and the 2A and 2B subdomains both have DNA binding sites, which makes it clear that these enzymes all share high structural homology (40%). Therefore, because they share common motifs, it is expected that all of the SF1 DNA helicases unwind DNA through a similar mechanism (21).

 Previous X-ray crystallographic studies suggested a dimeric helicase model for the complex of Rep and ssDNA (22) and a monomeric helicase model for the complex of PcrA and dsDNA with a 7-nt ssDNA tail (23). In these studies, real snapshots during the unwinding may not have been taken because ssDNA and not dsDNA was used for the analysis of Rep, as well as because the ssDNA length of the DNA substrate that was used for the study with PcrA was too short to allow multiple PcrA bindings and shorter than the length that has been found to be required for efficient DNA binding. Yang *et al.* investigated the binding stoichiometry of PcrA to the ssDNA length by quenching the intrinsic fluorescence of PcrA upon its binding to nucleic acids. They determined that the binding site size of PcrA was 9.3 ± 0.3 nt and the rates of the unwinding of the 5- and 10-nt ssDNA tails by PcrA were significantly lower than those obtained when a DNA with a longer tail was used (24). The size of the PcrA binding site was similar to that determined for UvrD (11 ± 1 nt (20) or 10 ± 2 nt (8)). In addition to the above structural studies, previous biochemical and single-molecule studies support the dimeric helicase model for Rep and PcrA and not for T4 Dda helicase (25). Oligomerization promotes the unwinding efficiency of Rep (26,27) and PcrA (24), In addition, a longer ssDNA tail increased the DNA unwinding efficiency of Rep and PcrA, which is similar to the effects that have been observed in single-turnover kinetics experiments of UvrD (3). Moreover, the Rep and PcrA helicases have been found to be processive ssDNA translocases in their monomeric form through single-molecule FRET experiments with Rep (28) and kinetic experiments with PcrA (29-31). However, these monomers fail to catalyze DNA unwinding. The single-molecule strategy employed in this study can therefore be used to address other monomer–dimer questions

regarding the mechanism of the SF1 helicases.

Supplementary References

1.   Ali, J. A., N. K. Maluf, and T. M. Lohman. 1999. An oligomeric form of *E. coli* UvrD is required for optimal helicase activity. *J. Mol. Biol.* 293:815-834.

2.   Maluf, N. K. and T. M. Lohman. 2003. Self-association equilibria of *Escherichia coli* UvrD helicase studied by analytical ultracentrifugation. *J. Mol. Biol.* 325:889-912.

3.   Maluf, N. K., C. J. Fischer, and T. M. Lohman. 2003. A dimer of *Escherichia coli* UvrD is the active form of the helicase *in vitro*. *J. Mol. Biol.* 325:913-935.

4.   Maluf, N. K., J. A. Ali, and T. M. Lohman. 2003. Kinetic mechanism for formation of the active, dimeric UvrD helicase-DNA complex. *J. Biol. Chem.* 278:31930-31940.

5.   Yokota, H., Y. W. Han, J.-F. Allemand, X. G. Xi, D. Bensimon, V. Croquette, and Y. Harada. 2009. Single-molecule visualization of binding modes of helicase to DNA on PEGylated surfaces. *Chem. Lett.* 38:308-309.

6.   Dessinges, M. N., T. Lionnet, X. G. Xi, D. Bensimon, and V. Croquette. 2004. Single-molecule assay reveals strand switching and enhanced processivity of UvrD. *Proc. Natl. Acad. Sci. USA* 101:6439-6444.

7.   Manosas, M., X. G. Xi, D. Bensimon, and V. Croquette. 2010. Active and passive mechanisms of helicases. *Nucleic Acids Res.* 38:5518-5526.

8.   Runyon, G. T., I. Wong, and T. M. Lohman. 1993. Overexpression, purification, DNA binding, and dimerization of the *Escherichia coli uvrD* gene product (helicase II). *Biochemistry* 32:602-612.

9.   Hermanson, G. T. 2008. Bioconjugate Techniques (2nd Edition): Academic Press.

10.   Lee, J. Y. and W. Yang. 2006. UvrD helicase unwinds DNA one base pair at a time by a two-part power stroke. *Cell* 127:1349-1360.

11.   Drapeau, G. R. 1980. Substrate specificity of a proteolytic enzyme isolated from a

mutant of *Pseudomonas fragi*. *J. Biol. Chem.* 255:839-840.

12.   Harada, Y., K. Sakurada, T. Aoki, D. D. Thomas, and T. Yanagida. 1990. Mechanochemical coupling in actomyosin energy transduction studied by *in vitro* movement assay. *J. Mol. Biol.* 216:49-68.

13.   Aitken, C. E., R. A. Marshall, and J. D. Puglisi. 2008. An oxygen scavenging system for improvement of dye stability in single-molecule fluorescence experiments. *Biophys. J.* 94:1826-1835.

14.   Lohman, T. M., K. Chao, J. M. Green, S. Sage, and G. T. Runyon. 1989. Large-scale purification and characterization of the *Escherichia coli rep* gene product. *J. Biol. Chem.* 264:10139-10147.

15.   Ali, J. A. and T. M. Lohman. 1997. Kinetic measurement of the step size of DNA unwinding by *Escherichia coli* UvrD helicase. *Science* 275:377-380.

16.   Sun, B., K. J. Wei, B. Zhang, X. H. Zhang, S. X. Dou, M. Li, and X. G. Xi. 2008. Impediment of *E. coli* UvrD by DNA-destabilizing force reveals a strained-inchworm mechanism of DNA unwinding. *EMBO J.* 27:3279-3287.

17.   Fischer, C. J., N. K. Maluf, and T. M. Lohman. 2004. Mechanism of ATP-dependent translocation of *E.coli* UvrD monomers along single-stranded DNA. *J. Mol. Biol.* 344:1287-1309.

18.   Tomko, E. J., C. J. Fischer, A. Niedziela-Majka, and T. M. Lohman. 2007. A nonuniform stepping mechanism for *E. coli* UvrD monomer translocation along single-stranded DNA. *Mol. Cell* 26:335-347.

19.   Tomko, E. J., C. J. Fischer, and T. M. Lohman. 2012. Single-stranded DNA translocation of *E. coli* UvrD monomer is tightly coupled to ATP hydrolysis. *J. Mol. Biol.* 418:32-46.

20.   Mechanic, L. E., M. C. Hall, and S. W. Matson. 1999. *Escherichia coli* DNA helicase II is active as a monomer. *J. Biol. Chem.* 274:12488-12498.

21. Lohman, T. M., E. J. Tomko, and C. G. Wu. 2008. Non-hexameric DNA helicases and translocases: mechanisms and regulation. *Nat. Rev. Mol. Cell Biol.* 9:391-401.

22. Korolev, S., J. Hsieh, G. H. Gauss, T. M. Lohman, and G. Waksman. 1997. Major domain swiveling revealed by the crystal structures of complexes of *E. coli* Rep helicase bound to single-stranded DNA and ADP. *Cell* 90:635-647.

23. Velankar, S. S., P. Soultanas, M. S. Dillingham, H. S. Subramanya, and D. B. Wigley. 1999. Crystal structures of complexes of PcrA DNA helicase with a DNA substrate indicate an inchworm mechanism. *Cell* 97:75-84.

24. Yang, Y., S. X. Dou, H. Ren, P. Y. Wang, X. D. Zhang, M. Qian, B. Y. Pan, and X. G. Xi. 2008. Evidence for a functional dimeric form of the PcrA helicase in DNA unwinding. *Nucleic Acids Res.* 36:1976-1989.

25. Nanduri, B., A. K. Byrd, R. L. Eoff, A. J. Tackett, and K. D. Raney. 2002. Pre-steady-state DNA unwinding by bacteriophage T4 Dda helicase reveals a monomeric molecular motor. *Proc. Natl. Acad. Sci. USA* 99:14722-14727.

26. Bjornson, K. P., M. Amaratunga, K. J. Moore, and T. M. Lohman. 1994. Single-turnover kinetics of helicase-catalyzed DNA unwinding monitored continuously by fluorescence energy transfer. *Biochemistry* 33:14306-14316.

27. Cheng, W., J. Hsieh, K. M. Brendza, and T. M. Lohman. 2001. *E. coli* Rep oligomers are required to initiate DNA unwinding *in vitro*. *J. Mol. Biol.* 310:327-350.

28. Myong, S., I. Rasnik, C. Joo, T. M. Lohman, and T. Ha. 2005. Repetitive shuttling of a motor protein on DNA. *Nature* 437:1321-1325.

29. Dillingham, M. S., D. B. Wigley, and M. R. Webb. 2000. Demonstration of unidirectional single-stranded DNA translocation by PcrA helicase: measurement of step size and translocation speed. *Biochemistry* 39:205-212.

30. Dillingham, M. S., D. B. Wigley, and M. R. Webb. 2002. Direct measurement of single-stranded DNA translocation by PcrA helicase using the fluorescent base analogue 2-aminopurine. *Biochemistry* 41:643-651.

31.   Niedziela-Majka, A., M. A. Chesnik, E. J. Tomko, and T. M. Lohman. 2007. *Bacillus stearothermophilus* PcrA monomer is a single-stranded DNA translocase but not a processive helicase *in vitro*. *J. Biol. Chem.* 282:27076-27085.